Published online 30 July 2015 *Nucleic Acids Research, 2015, Vol. 43, No. 17* **8283–8298**
doi: 10.1093/nar/gkv751

The RNA-binding protein HOS5 and serine/arginine-rich proteins RS40 and RS41 participate in miRNA biogenesis in Arabidopsis

Tao Chen, Peng Cui and Liming Xiong*

Division of Biological and Environmental Sciences and Engineering, King Abdullah University of Science and Technology (KAUST), Thuwal 23955-6900, Saudi Arabia

Received December 9, 2014; Revised July 8, 2015; Accepted July 11, 2015

ABSTRACT

MicroRNAs are a class of small regulatory RNAs that are generated from primary miRNA (pri-miRNA) transcripts with a stem-loop structure. Accuracy of the processing of pri-miRNA into mature miRNA in plants can be enhanced by SERRATE (SE) and HYPONASTIC LEAVES 1 (HYL1). HYL1 activity is regulated by the FIERY2 (FRY2)/RNA polymerase II C-terminal domain phosphatase-like 1 (CPL1). Here, we discover that HIGH OSMOTIC STRESS GENE EXPRESSION 5 (HOS5) and two serine/arginine-rich splicing factors RS40 and RS41, previously shown to be involved in pre-mRNA splicing, affect the biogenesis of a subset of miRNA. These proteins are required for correct miRNA strand selection and the maintenance of miRNA levels. FRY2 dephosphorylates HOS5 whose phosphorylation status affects its subnuclear localization. HOS5 and the RS proteins bind both intronless and intron-containing pri-miRNAs. Importantly, all of these splicing-related factors directly interact with both HYL1 and SE in nuclear splicing speckles. Our results indicate that these splicing factors are directly involved in the biogenesis of a group of miRNA.

INTRODUCTION

MicroRNAs, one of the small molecule RNA families, play critical roles in gene regulation in insects, plants and animals (1). After being transcribed by RNA polymerase II, primary miRNAs (pri-miRNAs) are processed into precursor miRNAs (pre-miRNAs) with a hairpin structure (2). Subsequently, pre-miRNAs are cut into miRNA/miRNA* duplexes and the miRNAs are then loaded into an Argonaut protein to guide the cleavage of target transcripts or to inhibit translation. In animals, pri-miRNAs are processed by RNase III Drosha into pre-miRNAs that are then cleaved into mature miRNAs by Dicer, another class of RNase III (3,4). Plants, however, lack Drosha homologs and instead use a single RNase III, DCL1 (Dicer-like 1) for both steps to generate miRNAs (5,6).

The efficient and accurate generation of miRNA requires a miRNA-processing complex that includes a dsRNA-binding protein, HYPONASTIC LEAVES 1 (HYL1); a zinc finger protein, SERRATE (SE); a G-patch domain-containing protein, TOUGH (TGH); and DCL1 (7–13). The balance of phosphorylation status of HYL1, which is regulated by the RNA polymerase II (RNPII) C-terminal domain (CTD) phosphatase FRY2 (also known as CPL1), is important for the accuracy of miRNA biogenesis (14). HEN1 performs the 2′-*O*-methylation of the miRNA/miRNA* duplex that is critical for its maturation and degradation (15,16). Several other components, such as cap-binding proteins CBP80/ABH1 and CBP20, the hydroxyproline-rich glycoprotein SICKLE (SIC), RNA binding protein MOS2, NOT2, PRL1, the DNA binding protein CDC5 and kinase RACK1 also have functions in miRNA processing (17–24). Most miRNA processing mutants of Arabidopsis have morphological or developmental defects, but others were found to have an altered sensitivity to stress; for example, *hyl1*, *se-1*, *abh1* and *sic-1* mutants are sensitive to salt stress and the stress hormone abscisic acid (ABA) (17,25–27).

Previous studies suggest that miRNA and mRNA processing may be closely related, as suggested by the involvement of the CBP80/ABH1 and CBP20 in both processes. Recent evidence adds components of RNA splicing to the interplay too. For instance, alternative splicing events have been found in SE mutants (28,29). STABILIZED1 (STA1), which is required for pre-mRNA splicing, is also involved in miRNA biogenesis (30,31) and AtGRP7, a protein involved in pre-mRNA processing, affects miRNA processing (32). Introns were also found to enhance the levels of miR163 in Arabidopsis (33,34). However, how splicing affects miRNA processing remains unclear.

We recently reported that HOS5, a RNA-binding protein with heterogeneous nuclear ribonucleoprotein (hnRNP) K homology (KH) domains, and two serine-arginine-rich

*To whom correspondence should be addressed. Tel: +966 12 808 2397; Email: liming.xiong@kaust.edu.sa

(SR) protein splicing factors, RS40 and RS41, are involved in pre-mRNA splicing. Here, we found that these proteins also participate in miRNA biogenesis. They all interact with microprocessor core proteins HYL1 and SE in co-immunoprecipitation (Co-IP), co-localization and bimolecular fluorescence complementation (BiFC) assays. HOS5, RS40 and RS41 proteins bind pri-miRNA *in vivo*. Using miRNA (miRNA-seq) and mRNA sequencing (RNA-seq), we found that not only the expression of many miRNAs was affected in *hos5*, *rs40* and *rs41* mutants, but the efficiency of miRNA cleavage was also affected. The transcript level of miRNA target genes changed accordingly to the level of disturbance to the miRNA in mutants. Together with other recent studies, our work establishes a direct link between mRNA splicing and miRNA biogenesis.

MATERIALS AND METHODS

Plant Materials

Arabidopsis thaliana plants were grown either in soil in a growth room or on Murashige and Skoog (MS) medium plates (solidified with 0.6% agar for horizontally placed plates and 1.2% agar for vertically placed plates) in a growth chamber at 21 ± 1°C on a 16/8 h of light/dark cycle. *hos5–1* and *fry2–1* mutants in the C24 background have previously been described (35,36). *hos5–2* (SALK_095666), *rs40–1* (WiscDsLox382G12) and *rs41–1* (SAIL_64_C03) are T-DNA insertion lines. *A hos5 rs40 rs41* triple mutant was generated by crossing *hos5–2*, *rs40–1* and *rs41–1*. HOS5 OX C24 and HOS5 OX *fry2–1* were transgenic plants overexpressing the FLAG-tagged HOS5 in the C24 (wild-type) and the *fry2–1* mutant background, respectively.

Vector construction

The cDNA of *HOS5*, *RS40*, *RS41*, *HYL1* and *SE* were amplified by RT-PCR and cloned into pENTR/D/TOPO (Invitrogen) to generate entry clones. For BiFC assays, all entry clones were transferred to the destination vectors nEYFP/pUGW2 and cEYFP/pUGW2 by LR recombination (37). For protein dephosphorylation assays, the entry clones of *HOS5*, *RS40* and *RS41* were introduced into pEarleyGate202 (38). For Co-IP, *HYL1* was inserted into pEarleyGate 202 and *HOS5*, *RS40* and *RS41* were transformed into pEarleyGate 203. For subcellular localization detecting by fluorescent protein, *HOS5* was inserted into pEarleyGate 101 and *HYL1* was transformed into pEarleyGate 101 and pGWB554 (39).

RNA analysis

For miRNA analyses, 12-day-old seedlings were ground in liquid nitrogen and total RNA was isolated by using PureLink Plant RNA Reagent (Ambion). Reverse transcription (RT) was performed by stem-loop RT using NCode EXPRESS SYBR GreenER miRNA qRT-PCR Kit (Invitrogen) as described (40). For mRNA analyses, total RNAs were extracted from 12-day-old seedlings using the RNeasy Plant Mini Kit (Qiagen), and the first-strand cDNAs were reverse transcribed by SuperScript III (Invitrogen). Quantitative RT-PCR was performed using the Applied Biosystems 7900HT Fast Real-Time polymerase chain reaction (PCR) system. *UBQ3* and *ACT2* were used as internal controls. Primers used are listed in Supplemental Table S6.

RNA sequencing and data analysis

RNA-seq libraries were constructed using the Illumina Whole Transcriptome Analysis Kit for mRNA-seq and the TruSeq Small RNA Sample Preparation Kit for miRNA-seq following the standard protocol (Illumina, HiSeq system) and sequenced on the HiSeq platform to generate high-quality single-end reads of 101 nucleotides (some with 85 nt due to machine failure) in length.

For microRNA sequencing, the software FastQc was used for evaluating the quality of the sequencing reads. The adaptor sequences were removed from the raw reads by Cutadapt. Bowtie was used to align the reads against the *Arabidopsis* genome sequences (downloaded from TAIR10) allowing 2 nt mismatches and the annotated miRNAs were obtained from the miRBASE database. miRNAs reads in a sample were normalized by the total reads of the sample. DEGseq was used to identify miRNAs with differential expressions. Fisher's Exact Test applied in the DEGseq was used to test for the significance for differentially expressed miRNAs (41).

TopHat (42) was used to align mRNA-seq reads against the Arabidopsis genome sequences and annotated gene models (downloaded from TAIR10, http://www.arabidopsis.org/) with default parameters. Genes with differential expression were identified by using the Cufflinks software (43).

To evaluate the accuracy of miRNA processing, the miRNA* regions of pri-miRNAs in the Arabidopsis genome were annotated based on the mature miRNA annotation, followed by reads counting of the miRNA and miRNA*. Three parameters were used to evaluate processing accuracy: (i) the absolute expression level of miRNA*, which was used to determine the change in the expression level of miRNA* in the mutant relative to that in the wild-type, (ii) the expression ratio of miRNA/miRNA* in a given sample, which was used to estimate the relative expression of miRNA* in that sample and (iii) the coverage of miRNA across the pri-miRNA loci in the genome as shown by Integrative Genomics Viewer (IGV) browser, which was used to illustrate the cleavage accuracy.

In vivo pri-miRNA binding assay

Five grams of fresh leaves per sample from seedlings at the rosette stage were harvested and protein–RNA was crosslinked by adding 1% formaldehyde and vacuumed for 15 min. The crosslink was stopped by adding 125 mM glycine and incubating for 5 min. Leaves were ground and resuspended in lysis buffer (100 mM KCl; 10 mM HEPES; 5 mM ethylenediaminetetraacetic acid (EDTA); 10% Glycerol; 0.1% NP-40; 200U/mL RNasin; 2 mM Ribonucleoside Vanadyl Complexes; 2 mM PMSF; 10 μl/ml protease inhibitor (PI, Sigma P9599)). RNA-IP was performed using anti-FLAG M2 beads with IgG beads as a control. After washing five times, the protein on the crosslinked complex was digested by proteinase K and the RNA was extracted with phenol–chloroform–isoamyl alcohol. Follow-

ing RT, real-time quantitative PCR was performed and the *ACT2* gene was used as a control.

Analysis of mRNA stability

Ten-day-old whole seedlings of HOS5 OX in C24 and HOS5 OX in *fry2–1* were incubated in half of the MS liquid medium containing 200 μM actinomycin D for 0, 4 and 8 h. Samples were harvested and total RNAs were extracted, followed by RT and real-time quantitative PCR as described above.

Protein analysis

For protein phosphorylation assays, total protein extracts were resuspended in lysis buffer (50 mM Tris–HCl (pH 7.9), 120 mM NaCl, 2 mM $MgCl_2$, 0.1% Triton X-100, 1 mM dithiothreitol (DTT), 2 mM PMSF, 1× PIs (Sigma P9599), 10% Glycerol). The samples were aliquoted for control and CIP treatments (4 and 8 h, respectively). All samples were loaded onto a Phos-tag polyacrylamide gel electrophoresis (PAGE) gel or regular PAGE gel and transferred to polyvinylidene fluoride (PVDF) membranes. Signals were detected by the anti-FLAG M2 antibody.

Protein Co-IP, BiFC and co-localization assays were performed in protoplasts. Arabidopsis protoplasts were isolated and a polyethylene glycol (PEG)-mediated transformation was performed by standard protocols. Briefly, cell walls were removed using fungal cellulase R10 and macerozyme R10, resulting in the release of protoplasts. Constructs were transformed into protoplasts by PEG-calcium transfection. After 16 h of incubation at room temperature, cells were harvested for further analysis as described below.

For co-immunoprecipitation assay, the above cells were resuspended in IP buffer (100 mM KCl; 10 mM HEPES; 2 mM EDTA; 10% Glycerol; 0.1% NP-40; 2 mM PMSF; 1× PIs). After centrifugation, the supernatants were transferred to new tubes. The samples were precleaned by adding normal IgG-conjugated beads and then divided into two groups. IgG beads and M2 beads were then added into the respective groups. After 3 h of incubation, the beads were washed five times with the lysis buffer. All samples were loaded to Sodium dodecyl sulphate-polyacrylamide gel electrophoresis (SDS-PAGE) gels and transferred to PVDF membranes. Signals were detected by anti-FLAG M2 and anti-c-Myc antibodies.

For BiFC and co-localization assays, cells were suspended in WI buffer (4 mM MES (pH 5.7), 0.5 M mannitol, 20 mM KCl). Signals of fluorescent proteins were detected with a LSM 710 inverted confocal microscope (Carl Zeiss).

GUS staining

Promoters of *RS40* and *RS41* (1.6 Kb) were amplified from genomic DNA of *Arabidopsis* (ecotype Columbia) and ligated to the pENTR vector. The promoters were cloned into the destination vector pMDC162 and then transformed into the *Agrobacterium tumefaciens* strain GV3101. Transgenic plants were generated by flower dipping and screened on the MS selection medium. For β-glucuronidase (GUS) analysis, samples from different stages of seedlings and different parts of adult plants were immersed in GUS staining buffer at 37°C overnight and then destained with 75% ethanol.

RESULTS

HOS5 is dephosphorylated by FRY2

We recently showed that the KH-domain RNA-binding protein HOS5 interacts with the RNA polymerase II CTD phosphatase-like protein FIERY2 (FRY2)/CPL1 and that the localization of HOS5 was altered in the *fry2* mutant (44). Since FRY2 is a phosphatase, a logical hypothesis for the relevance of this interaction would be that FRY2 dephosphorylates HOS5 and that the phosphorylation status of HOS5 determines its subnuclear localization. To test this hypothesis, we constructed a binary vector of FLAG-tagged HOS5 and transformed it into Arabidopsis wild-type (ecotype C24) and the *fry2–1* mutant. The T_2 generation of the transgenic plants, named as HOS5 OX C24 and HOS5 OX *fry2–1,* respectively, were obtained. Using Phos-tag, a compound that decreases the mobility of phosphorylated proteins in polyacrylamide gels (45), we conducted western blot analyses with crude proteins extracted from the transgenic plants.

As shown in Figure 1A, there were two bands of HOS5 on the Phos-tag gel: the upper band likely represents the phosphorylated form (HOS5-P) and the lower band the unphosphorylated form. To verify that the two bands differ in their phosphorylation status, whole protein extract from the HOS5 OX *fry2–1* plants was treated with CIP (Alkaline Phosphatase, Calf Intestinal) for 4 or 8 h before being subjected to electrophoresis on Phos-tag or non-Phos-tag gels. The amount of protein in the non Phos-tag control gel was not significantly affected by CIP treatments, however, the amount of the protein in the upper bands of the Phos-tag gel decreased, while that in the corresponding lower bands increased (Figure 1A), confirming that the upper band is indeed phosphorylated HOS5.

Compared with HOS5 OX C24 plants, the amount of phosphorylated HOS5 relative to unphosphorylated HOS5 in the HOS5 OX *fry2–1* increased significantly (Figure 1A). Interestingly, the level of total HOS5 protein (both phosphorylated and unphosphorylated) was also higher in HOS5 OX *fry2–1* plants than in HOS5 OX C24 plants, as indicated by western blot analyses of these samples subjected to non-Phos-tag gel electrophoresis (Figure 1A). This increased level of the HOS5 protein in HOS5 OX *fry2–1* relative to HOS5 OX C24 plants could have resulted from transcriptional, post-transcriptional or post-translational regulation of the HOS5 gene or the protein.

To understand the possible cause for the enhanced accumulation of the HOS5 protein in the *fry2–1* mutant background, we first examined the RNA level of the *HOS5* gene in transgenic plants and control plants. The transcript level of *HOS5* was higher in *fry2–1* than in the wild-type C24 (Supplementary Figure S1A). In the two transgenic plants, the transcript levels of both the endogenous *HOS5* gene and the transgenic *HOS5* gene were higher in HOS5 OX *fry2–1* than in HOS5 OX C24 (Supplementary Figure S1B). Since the level of *HOS5* mRNA (Supplementary Figure

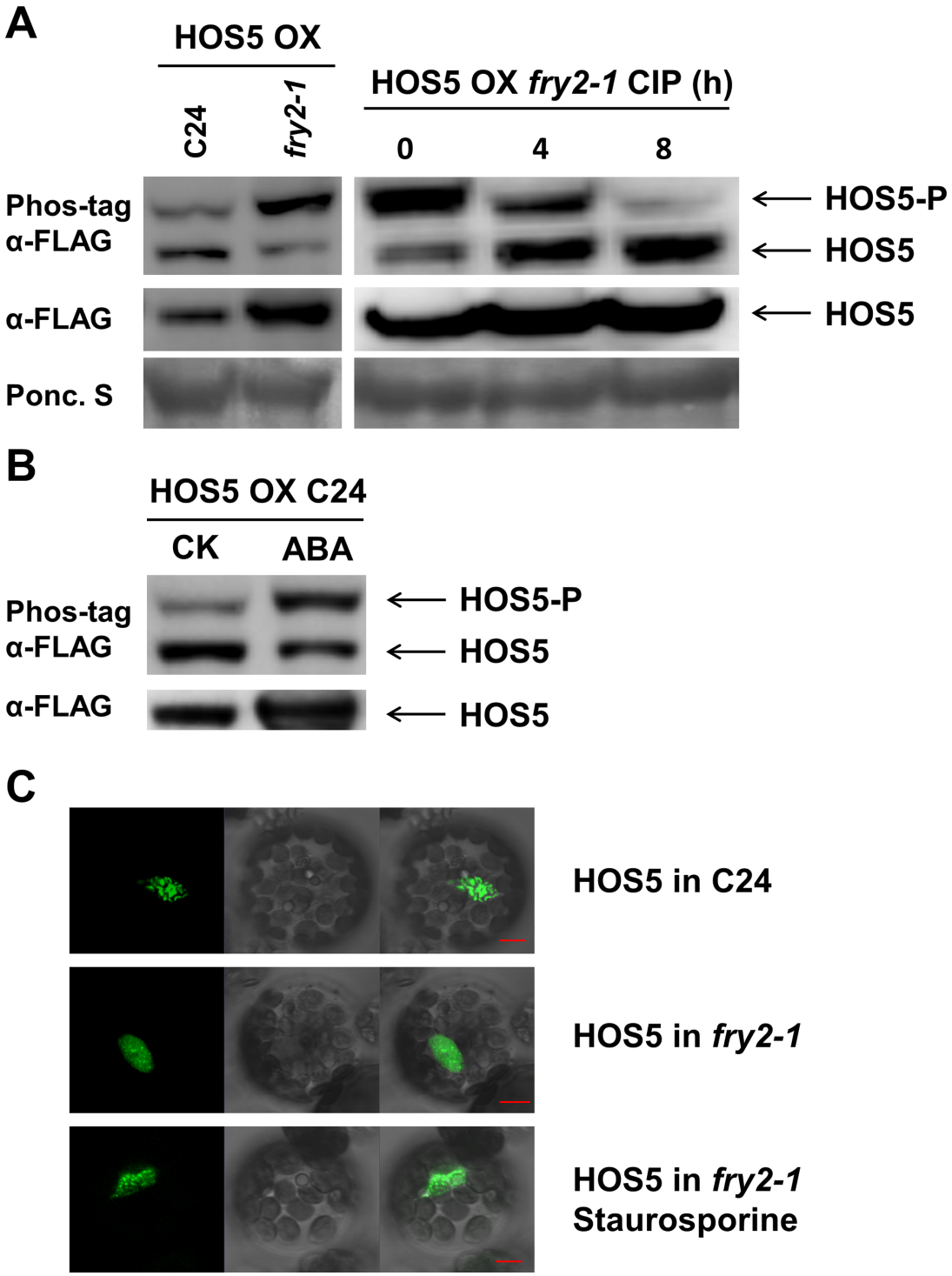

Figure 1. HOS5 is dephosphorylated by FRY2. (**A**) Phosphorylation status of HOS5 is controlled by FRY2. Left panels: proteins were extracted from 12-day-old HOS5 OX C24 and HOS5 OX *fry2–1* seedlings and separated on SDS-PAGE gel containing Phos-tag. The phosphorylated (HOS5-P) and unphosphorylated (HOS5) bands of HOS5 were detected by anti-FLAG antibody (Phos-tag α-FLAG). Proteins separated on regular SDS-PAGE gel were used as a loading control (α-FLAG). Right panels: proteins were extracted from 12-day-old HOS5 OX *fry2–1* seedlings and treated with calf intestinal alkaline phosphatase (CIP) for 0, 4 and 8 h. HOS5 proteins were detected as described above. Ponc.S, Ponceau S staining was used as a loading control. (**B**) Phosphorylation status of HOS5 under ABA treatment. HOS5 OX C24 plant seedlings were treated with ABA for 0 (CK) or 3 h (ABA). Proteins were extracted and separated on Phos-tag SDS-PAGE (upper panel) or on regular SDA-PAGE (lower panel) gels and detected as described in (A). (**C**) Mis-localization of HOS5 in *fry2–1* was rescued by the protein kinase inhibitor staurosporine. Left panels, GFP signals; middle panels, bright field images; right panels, merged images. HOS5 OX C24 and HOS5 OX *fry2–1*, flag-tagged HOS5 was over-expressed in the wild-type (C24) and in the *fry2–1* mutant, respectively; HOS5 in C24, GFP-tagged HOS5 was transiently expressed in C24 protoplasts; HOS5 in *fry2–1*, GFP-tagged HOS5 was transiently expressed in *fry2–1* protoplasts; HOS5 in *fry2–1* Staurosporine, GFP-tagged HOS5 was transiently expressed in *fry2–1* protoplasts with staurosporine treatment. Scale bars = 5 μm.

S1B) correlated with the level of protein expression (Figure 1A) in the two transgenic plant lines, we posited that the expression of HOS5 was regulated transcriptionally or post-transcriptionally rather than post-translationally. Since the endogenous *HOS5* promoter and the promoter for HOS5 overexpression (i.e. cauliflower mosaic virus 35S) are very different and may be regulated differently, yet both endogenous HOS5 and transgenic HOS5 transcripts accumulated similarly, we reasoned that the *HOS5* transcript may have altered stability in the *fry2* mutant background. After treatment with the transcription inhibitor actinomycin D for 0, 4 and 8 h, the transcript levels of *HOS5* in the two transgenic lines were examined by quantitative real-time PCR. As can be seen in Supplementary Figure S1C, the transgenic HOS5 mRNA degraded more rapidly in HOS5 OX C24 than in HOS5 OX *fry2–1*, whereas the degradation rate of a reference gene *ACT2* was similar between samples (Supplementary Figure S1D). Thus, the higher level of HOS5 protein in HOS5 OX *fry2–1* may mainly result from an increased stability of *HOS5* transcripts in the *fry2* mutant background.

Since the *hos5* mutant is hypersensitive to the stress hormone ABA (35), we also examined the phosphorylation level of HOS5 under ABA (200 μM ABA, 3 h) treatment. Results showed that the ratio of phosphorylated to unphosphorylated HOS5 and the total amount of the protein increased in response to ABA treatment (Figure 1B).

Given that HOS5 was dephosphorylated by FRY2 and that we previously observed an altered localization of HOS5 in the *fry2* mutant (44), we next asked whether the phosphorylation status of HOS5 would affect its localization. We fused in frame green fluorescent protein (GFP) with HOS5 at its C-terminus and transiently expressed the construct into C24 and the *fry2–1* mutant protoplasts by using a PEG-mediated method (46). Transformed *fry2–1* cells were divided into two aliquots, one with and one without treatment of staurosporine, a protein kinase inhibitor. After 16 h of incubation in a growth chamber, GFP signals were examined under a ZEISS LSM710 inverted confocal microscope. HOS5 was localized in the nuclear speckles in C24 (upper panels, Figure 1C) but was diffused throughout the nucleoplasm in the *fry2–1* mutant (middle panels, Figure 1C), similar to what we previously reported (44). Strikingly, the localization pattern of HOS5 in the *fry2–1* mutant was completely rescued by being treated with 1 μM of staurosporine. Taken together, these data demonstrated that FRY2 could dephosphorylate HOS5 and that phosphorylation status may affect the subnuclear localization of HOS5.

In our previous study, we found that HOS5 and FRY2 also interacted with two splicing factors, RS40 and RS41, and that these two splicing factors played important roles in pre-mRNA splicing. To address whether FRY2 could also dephosphorylate these two splicing factors, we made plant binary vectors by fusing the FLAG tag at the C-termini of RS40 and RS41 and transformed these constructs respectively into wild-type and *fry2–1* mutant plants to generate stable transgenic plants. The phosphorylation status of RS40 and RS41 were examined in T_2 transgenic plants by western blot analysis of the phosphorylated proteins on the Phos-tag gel and the total proteins on the non-Phos-tag PAGE gel as a control. RS40 and RS41 were similarly phosphorylated and little difference in the phosphorylation level was apparent between the C24 and *fry2–1* plants (Supplementary Figure S2A). It is thus likely that FRY2 is not the major phosphatase that dephosphorylates RS40 and RS41.

FRY2 has been demonstrated as a regulator of miRNA processing by balancing the phosphorylation level of HYL1 (14). We asked whether FRY2 also affects HYL1 localization as it does on HOS5. A construct of HYL1 fused with GFP was transiently expressed in C24 and *fry2–1* protoplasts. Half of the *fry2–1* transformed cells were treated with staurosporine. After incubation for 16 h, GFP signals were examined in about 200 cells for each treatment, and the images of the representative cells are shown in Supplementary Figure S2B. In C24 cells, HYL1-GFP signals could be seen in the entire nuclei but were more concentrated in two to three nuclear bodies (Supplementary Figure S2B). In *fry2–1*, however, the number of nuclear bodies with HYL1-GFP within the cells decreased (Supplementary Figure S2B and C). Interestingly, staurosporine treatment of *fry2–1* cells rescued the number of HYL1-GFP-containing nuclear bodies to the wild-type level. The difference between the wild-type C24 and *fry2–1* in the number of HYL1-GFP-containing bodies was statistically significant (Supplementary Figure S2C). These data indicated that, like HOS5, the phosphorylation level of HYL1 might also affect its subnuclear localization. This observation is consistent with the observation that HYL1 phosphorylation status affects the formation of HYL1-containing nuclear bodies (14).

HOS5, RS40 and RS41 interact with HYL1 and SE in splicing speckles

The above data suggest that there is a certain similarity in the regulation of HOS5 and HYL1 by FRY2. This prompted us to investigate whether HOS5, RS40 and RS41 physically associate with HYL1. After co-transforming FLAG-tagged HYL1 with c-Myc-tagged HOS5, RS40 and RS41 into *Arabidopsis* protoplast cells, we performed Co-IP using anti-FLAG M_2 beads. All three proteins, HOS5, RS40 and RS41, were pulled down by HYL1 (Figure 2A), indicating that HYL1 interacts with these proteins *in vivo*.

To examine whether the HYL1 protein co-localized with HOS5, RS40 and RS41, we made constructs of HYL1-mRFP, HOS5-GFP, RS40-GFP and RS41-GFP. The HYL1-mRFP plasmid was co-transformed with each of the other plasmids into protoplasts. Consistent with previous studies, HYL1 was particularly accumulated in miRNA processing bodies (8) and HOS5 was found in splicing speckles (44) (Supplementary Figure S3A–C). The two splicing factors, RS40 and RS41, were also localized in the nuclei; yellow signals represent the overlapping localization of HYL1 and the other proteins (Supplementary Figure S3A–C).

We verified the results of Co-IP and co-localization studies by performing BiFC assays using the N-terminus of YFP (N-YFP) and the C-terminus of YFP (C-YFP) fused to these proteins; these constructs were then transferred into *Arabidopsis* protoplasts. After 16 h of incubation, the samples were examined for YFP signals under a confocal microscope. We found that HYL1 interacts with HOS5, RS40 and RS41 *in vivo*, and the interaction occurred in

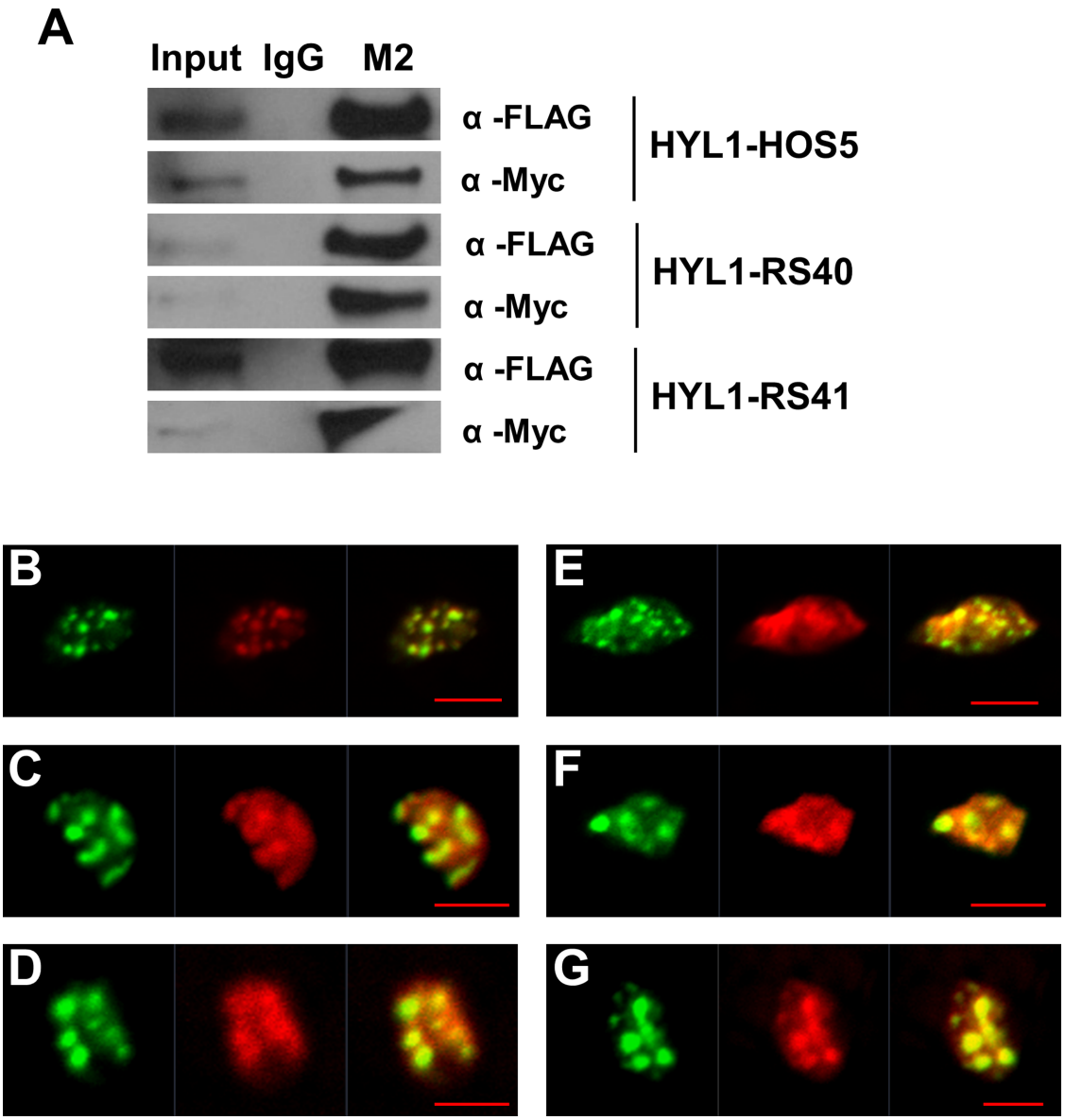

Figure 2. HOS5, RS40 and RS41 interact with HYL1 and SE *invivo*. (**A**) Co-IP of HYL1 with HOS5, RS40 and RS41. The plasmids for HYL1-FLAG, HOS5-Myc, RS40-Myc and RS41-Myc fusion protein were transiently expressed in Arabidopsis protoplasts. Proteins were immunoprecipitated from total protein extracts with anti-FLAG M2 beads (IgG used as control) and analyzed by immunoblots with anti-FLAG M2 antibody to detect HYL1-FLAG and anti-Myc antibody to detect HOS5, RS40 and RS41. (**B**–**G**) Co-localization of BiFC signals with the splicing speckle marker CypRS64. Plasmids of CypRS64-mRFP and BiFC combinations of plasmids HYL1-HOS5 (B), HYL1-RS40 (C), HYL1-RS41 (D), SE-HOS5 (E), SE-RS40 (F) or SE-RS41 (G). BiFC (left), CypRS64 (middle) and merged (right) signals are shown. Scale bars = 1 μm.

nuclear speckles (Supplementary Figure S3D). To confirm that these speckles were splicing speckles, we monitor the splicing speckles marker CypRS64-mRFP (44,47) for co-localization with the BiFC signals. Indeed, the interacting signals of HYL1 and HOS5 co-localized with the splicing speckle marker (Figure 2B). Similarly, both HYL1-RS40 and HYL1-RS41 BiFC signals co-localized with CypRS64-mRFP signals (Figure 2C and D). In summary, HYL1 interacts with HOS5, RS40 and RS41 in splicing speckles.

Since HYL1 interacts with another important component of miRNA processing complex, SE (12), we hypothesized that SE might interplay with HOS5 and the two splicing factors. These proteins were tagged with N-YFP and introduced with C-YFP tagged SE into protoplasts to perform BiFC assays. We observed that SE interacts with HOS5, RS40 and RS41. Furthermore, the patterns of interaction sites were similar to those with HYL1 (Supplementary Figure S3E). The co-localization of the BiFC signals with the CryRS64-mRFP signals indicated that these were also the nuclear splicing speckles (Figure 2E–G). Therefore, HOS5, RS40 and RS41 also interact with SE *in vivo* in splicing speckles.

HOS5, RS40 and RS41 are required for miRNA biogenesis

Given that the three pre-mRNA splicing-related proteins HOS5, RS40 and RS41 interact with three important miRNA biogenesis proteins, namely, HYL1, SE and FRY2/CPL1, we asked whether HOS5, RS40 and RS41 are involved in miRNA processing. Due to the high homology and redundancy between the RS40 and RS41 proteins, we used the *rs40 rs41* double mutant (44) to investigate the impacts of these proteins on miRNA expression. We performed miRNA-sequencing (miRNA-seq) with the *hos5–1,* the *rs40 rs41* double mutant and the wild-types C24 and Columbia (Col) seedlings using the Illumina Hi-seq platform. The quality scores of the sequencing reads were quite high (Supplementary Figure S4A–D).

It has been suggested that mutations of *FRY2* and *HYL1* lead to misprocessing of miRNA, as represented by incorrect strand selection (i.e. an aberrant accumulation of the miRNA passenger/complementary strand, miRNA*) (14). To establish whether this misprocessing occurred in the *hos5–1* and *rs40 rs41* mutants, we aligned the sequencing reads to each miRNA locus (total 270 annotated miRNA loci from the miRBASE database) and found that the number of misprocessed reads that were mapped to the 'miRNA*' strand of pre-miRNA was greater in the *hos5–1* mutant. In total, 29 miRNA loci accumulated more 'miRNA*' reads (mutant/wild-type > 1.5× at the expression level) in the *hos5–1* mutant and 9 miRNA loci in the *rs40 rs41* mutant (Figure 3A and Supplementary Tables S1 and S2). Of the loci identified by miRNA-seq, many were shared by the two mutants. We checked the miRNA and miRNA* levels in three loci by stem-loop real-time RT-PCR miRNA assays (40). Using the ratio of miRNA/miRNA* to represent the efficiency of miRNA processing, we found that the miRNA processing efficiencies of three selected miRNAs, miR162a, miR391 and miR169a, were significantly reduced in *hos5–1* and *rs40 rs41* mutants (Figure 3B–E). As shown by IGV browsers (Figure 3F and G), the expression level of miR162* increased significantly in *hos5* and *rs40 rs41* mutants relative to that in the corresponding wild-types. A similar accumulation of the passenger strands of four other representative loci, miR170, miR173–5p, miR825 and miR830 was also confirmed in these mutants (Supplementary Figure S4E–H).

Next, we examined whether HOS5 affects the expression of mature miRNA. By comparing the read counts at the 270 miRNA loci between mutants and the wild-type, we identified 73 and 47 miRNA that were differentially expressed (P-value < 0.01), accounting for 27.0 and 17.4% of the total miRNA in *hos5–1* and *rs40 rs41* mutants, respectively (Figure 4A, Supplementary Tables S3 and S4). Among these differentially regulated miRNAs, 34 were shared by both mutants (Figure 4B). The expression levels of three of these miRNAs, miR399, miR390 and miR827, were visualized as examples by IGV browser (Figure 4C–E) and were validated by stem-loop real-time RT-PCR miRNA assays (Figure 4F–H).

To confirm that the above miRNA phenotypes in the *hos5–1* and the *rs40 rs41* mutants were caused by HOS5, RS40 and RS41, we analyzed the miRNA/miRNA* ratios and mature miRNA expression levels in HOS5 + *hos5–1* (the complementation line of the *hos5–1* mutant) as well as *rs40* and *rs41* mutants, which were used as single gene complementation lines of the *rs40–rs41* double mutant. As shown in Supplementary Figure S5, the miRNA/miRNA* ratios and mature miRNA levels were restored close to the wild-type levels by wild-type HOS5, RS40 and RS41 in the mutants.

We further examined the accuracy of miRNAs cleavage in *hos5–1* and *rs40 rs41* mutants. Results showed that 12 miRNAs were mis-cleaved in the *hos5–1* mutant, but none were found mis-cleaved in the *rs40 rs41* mutant, indicating that HOS5 has additional roles in the accurate processing of a subset of miRNAs. The miRNA reads at all the twelve loci were aligned against these loci and visualized by the IGV browser, which showed that some of these miRNAs were from non-miRNA-coding regions in the *hos5* mutant (Supplementary Figure S6, Table S5). Considering the inaccuracy of miRNA processing in *hos5–1* but not in the *rs40 rs41* mutant, and that HOS5 and HYL1 could but RS40 and RS41 could not be dephosphorylated by FRY2, we propose that HOS5 ensures the accuracy of miRNA processing, likely by working together with FRY2 and HYL1.

Given the defects in miRNA biogenesis and expression in *hos5–1* and *rs40 rs41* mutants, we examined expression levels of miRNA biogenesis-related genes in these mutants. Compared to the wild-type, these mutants had a higher expression level of *FRY2*, lower expression levels of *SE*, *CBP20* and *HEN1* and a similar expression level of *ABH1*/*CBP80* (Supplementary Figure S7).

pri-miRNA splicing and expression as affected by HOS5, RS40 and RS41

We investigated whether HOS5, RS40 and RS41 are involved in pri-miRNA splicing. A previous study reported 12 intron-containing miRNA genes (48). Using RT-PCR, we checked the splicing of these intron-containing miRNA genes. Whereas most of these miRNA genes did not have significant change in the intron splicing (data not shown), introns in pri-miRNA 156a and pri-miRNA 157c were significantly retained in *hos5* and *rs40 rs41* mutants compared with the wild-type (Figure 5A). This finding suggested that HOS5, RS40 and RS41 may participate in the splicing of these pre-miRNAs. Furthermore, the levels of mature miRNA 156a and 157c were downregulated in these mutants (Figure 5B), suggesting that abnormal processing of pre-miRNA 156a and 157c may affect their mature miRNA expression. Nonetheless, for the other pri-miRNA whose splicing was not affected, there was no consistent pattern of miRNA expression among these mutants. In fact, either increased, decreased or unchanged levels of mature miRNA could be found in the *hos5* or *rs40 rs41* mutants relative to the wild-type (Supplementary Tables S3 and S4).

RS40 and *RS41* are predominantly expressed in roots

The general expression of the *RS40* and *RS41* genes in different parts of the plant was reported in an early study (49) yet their expression at the tissue level had been unknown. To examine the expression pattern of *RS40* and *RS41* genes, we conducted promoter reporter assays. Constructs consisting of the 1.5-kb promoter regions upstream

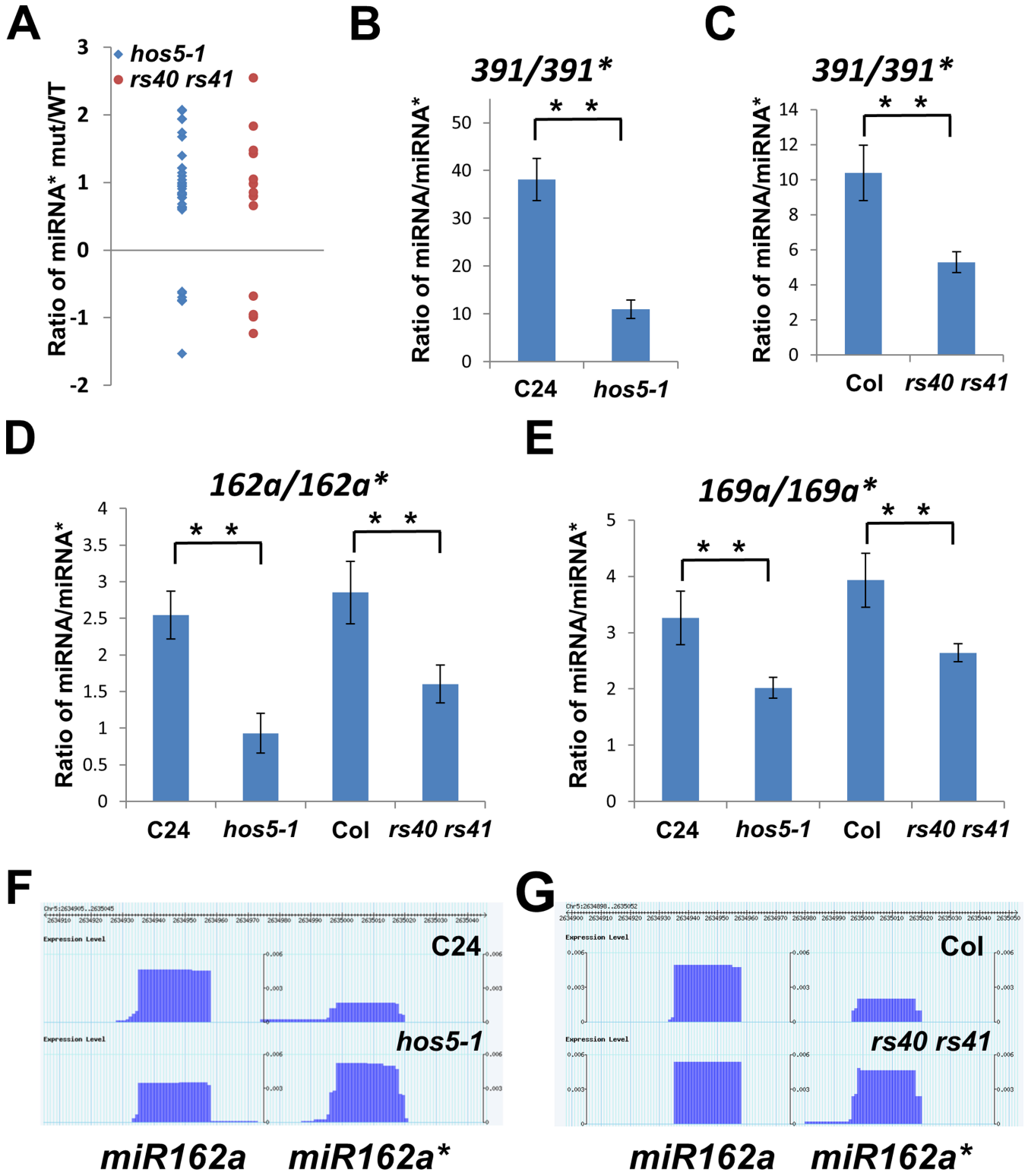

Figure 3. Difference of miRNA processing efficiency between wild-type and mutants. (**A**) The ratio of miRNA* expression level in mutants to wild-type (WT) in the *hos5–1* and *rs40 rs41* at different loci. (**B**–**E**) miRNAs processing efficiency, represented by the ratio of miRNA/miRNA*, of three miRNAs in *hos5–1* and *rs40 rs41* validated by microRNA stem-loop quantitative RT-PCR. Data are means and standard deviation ($n = 6$). Asterisks indicate a significant difference between the indicated samples (*t*-test, $^{**}P < 0.01$). (F and G) The expression levels of the miR162a and miR162a* in wild-types, *hos5–1* and *rs40 rs41* were shown by IGV browser.

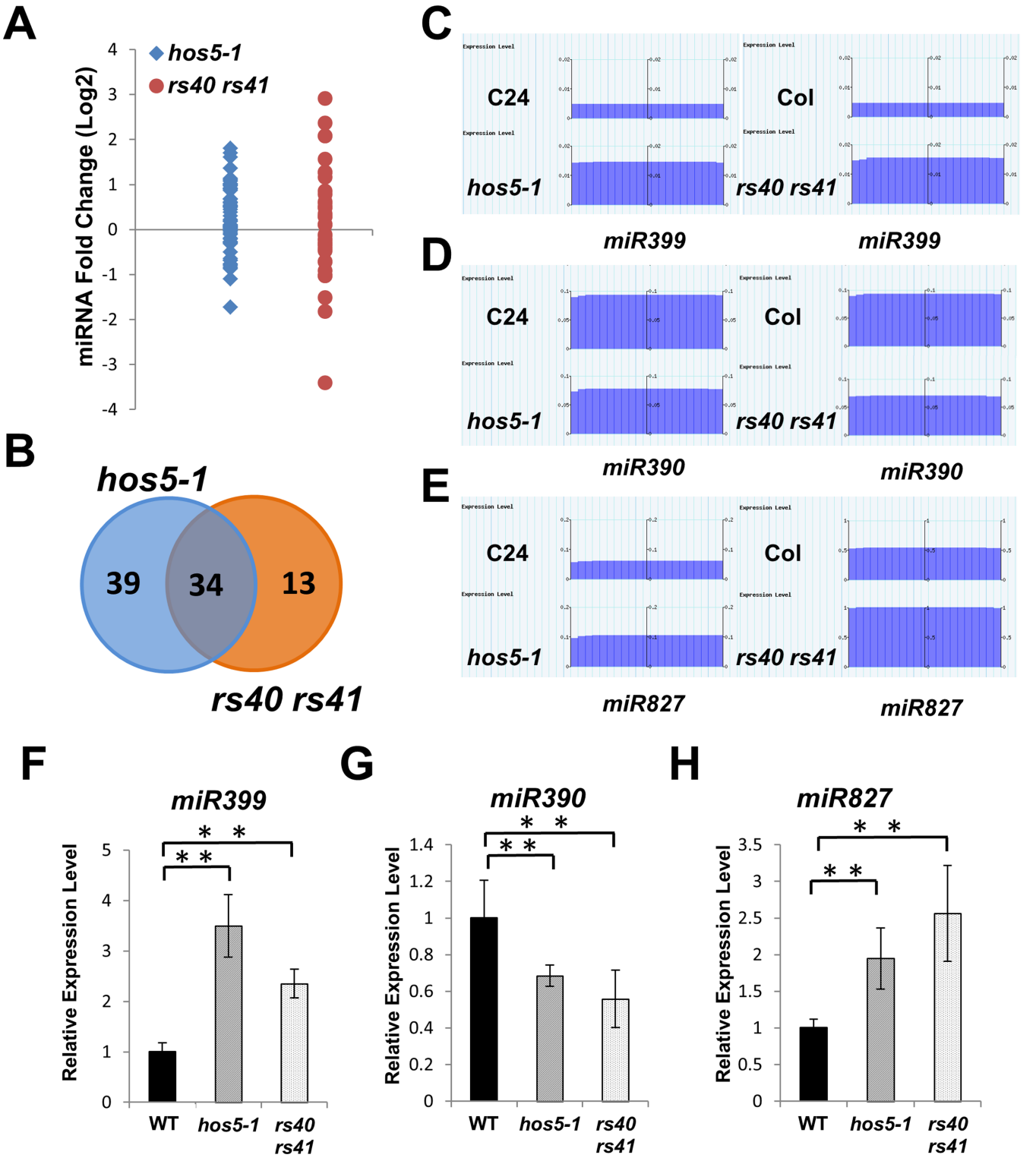

Figure 4. Expression of miRNAs in *hos5* and *rs40 rs41* mutants. (**A**) The fold change (mutant/WT) of the expression level of miRNAs that showed significantly differential expression in the *hos5–1* and *rs40 rs41* mutants relative to the wild-types. (**B**) Comparison of the numbers of differentially expressed miRNAs in *hos5–1* and *rs40 rs41* mutants. (**C**–**E**) Expression levels of the miRNA from the loci miR399, miR390 and miR827 as shown by IGV browser. (**F**–**H**) Validation of the miRNA expression in *hos5–1* and *rs40 rs41* mutants relative to the wild-types by microRNA stem-loop quantitative RT-PCR. Data are means and standard deviation ($n = 6$). WT, wild-type (C24 for *hos5–1* and Col for *rs40 rs41*). Asterisks indicate a significant difference between the indicated samples (*t*-test, $^{**}P < 0.01$).

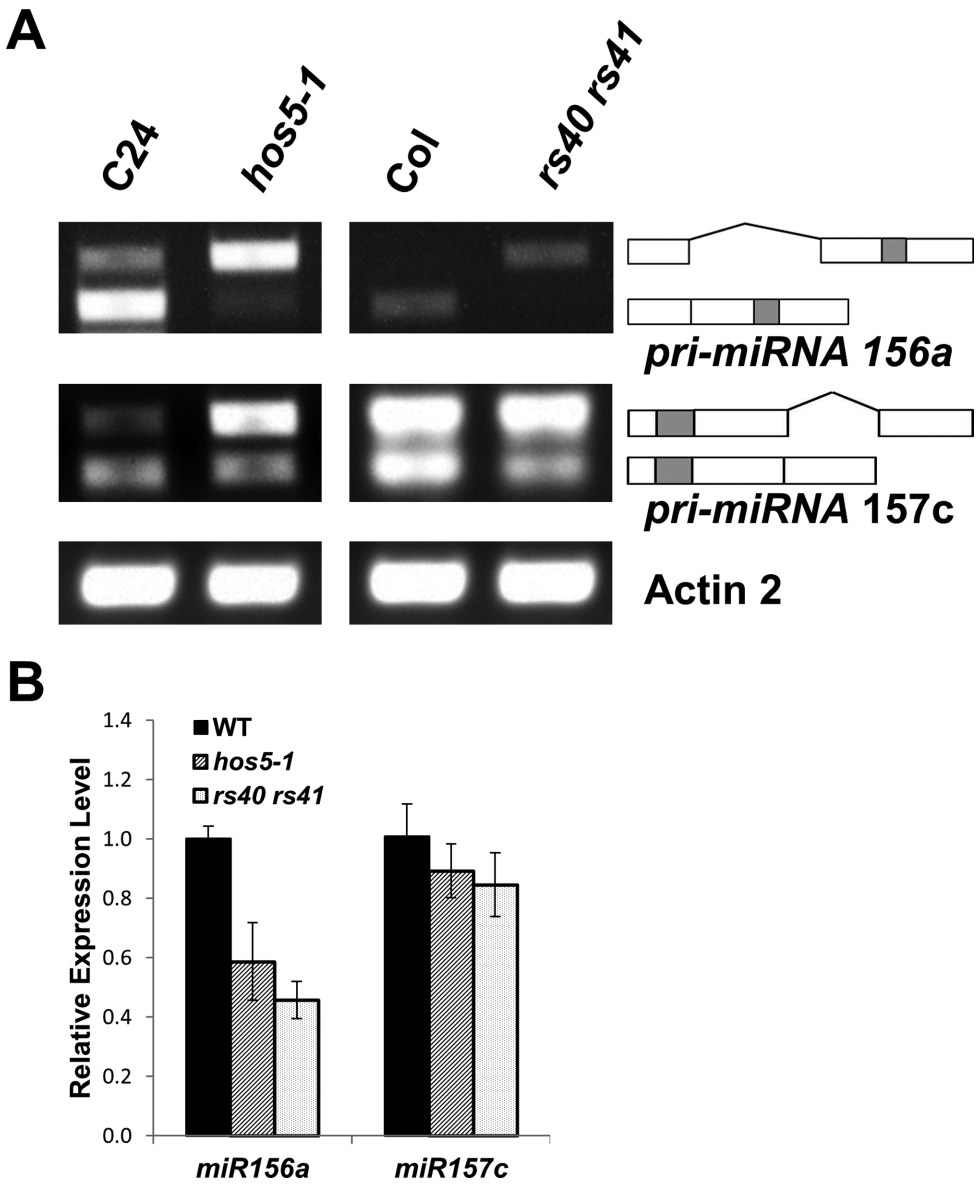

Figure 5. pri-miRNA splicing defects in *hos5* and *rs40 rs41* mutants. (**A**) Intron retention events in pri-miRNA in *hos5–1*, *rs40 rs41* and the corresponding wild-types. *ACTIN2* was used as a control. The paradigms of pri-miRNAs are shown to the right and checked introns are marked as fold lines. (**B**) The relative expression level of miRNA in the wild-types, *hos5–1* and *rs40 rs41* seedlings, measured by microRNA stem-loop quantitative RT-PCR. Error bars represent the standard deviation ($n = 6$).

of the ATG start codon of *RS40* and *RS41* fused to the β-glucuronidase (*GUS*) reporter gene were transformed into Col-0 plants. GUS expression was stained in these transgenic lines. In 5-day-old seedlings expressing *RS40* promoter-*GUS*, a strong GUS signal was predominantly detected in roots (Figure 6A). Increased expression of the gene was evident particularly at the root apical meristem and shoot apical meristem compared to other parts of the root and shoot (Figure 6B and C). The expression pattern of 8-day-old seedlings (Figure 6D) is similar to that of 5-day-old seedlings (Figure 6A). GUS expression was seen in root hairs, root vascular tissues, root tip, leaf primordia and lateral root primordia (Figure 6E–H). In 14-day-old seedlings, the GUS signal remained strong in root and leaf promordia (Figure 6I and J). The expression pattern of *RS41* was similar to that of *RS40*, as shown for seedlings of 5-day old (Figure 6K–M), 8-day-old (Figure 6N–R) and 14-day-old (Figure 6S and T) seedlings. In adult plants, both *RS40* and *RS41* were expressed strongly in flowers, especially in pollens and stigmas. No GUS signals were detected in stems and seeds (Supplementary Figure S8).

The *hos5 rs40 rs41* mutant is hypersensitive to auxin and has higher levels of miR160 and miR167

Despite the importance of their roles in RNA processing and gene regulation, our previous studies found only relatively mild stress-related phenotypes of the *fry2*, *hos5*, *rs40* and *rs41* single mutants (35,36,44). For this reason, we generated a *hos5 rs40 rs41* triple mutant. Based on the ex-

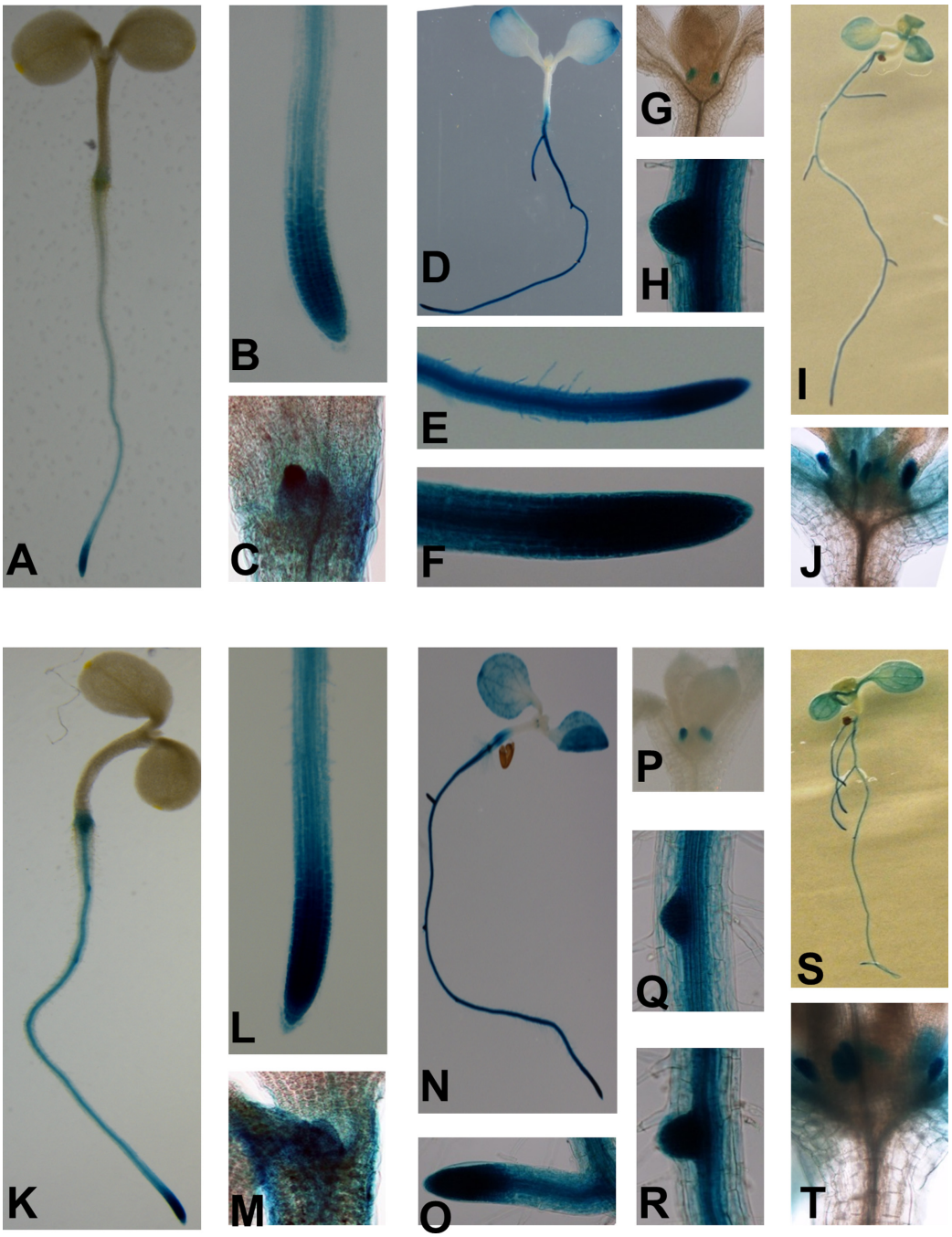

Figure 6. Expression patterns of *RS40* and *RS41* in seedlings. (**A**–**J**) *RS40* promoter-GUS activities in seedlings. (A–C) Five-day-old seedlings. Whole seedling (A), primary root tip (B) and leaf primordium (C). (D–H) Eight-day-old seedlings. Whole seedling (D), lateral root (E), primary root tip (F), leaf primordium (G) and emerging lateral root (H). (I and J) Fourteen-day-old seedlings. Whole seedling (I) and leaf primordium (J). (**K**–**T**) *RS41* promoter-GUS activities in seedlings. (K–M) Five-day-old seedling. Whole seedling (K), primary root tip (L) and leaf primordium (M). (N–R) Eight-day-old seedlings. Whole seedlings (N), lateral root (O), leaf primordium (P) and emerging lateral root (Q and R). (S and T) Fourteen-day-old seedlings. Whole seedling (S) and leaf primordium (T).

pression patterns of HOS5, RS40 and RS41, we expected that the triple mutant might have some phenotypes in the roots at the seedling stage. Indeed, we noticed that the triple mutants appeared to have slightly more lateral roots, implicating an altered auxin physiology. We tested the auxin response of the triple mutant by transferring 5-day-old seedlings to auxin-containing MS medium. As shown in Figure 7A, on MS medium without auxin, both the lateral root numbers and average length were slightly higher in *hos5 rs40 rs41* than in the wild-type. In the presence of 10 nM indole acetic acid (IAA) the difference became significant. After the plates were placed horizontally for 2 days, the root tips of the triple mutants showed more dramatic root-curling than those of the wild-type (Figure 7B), indi-

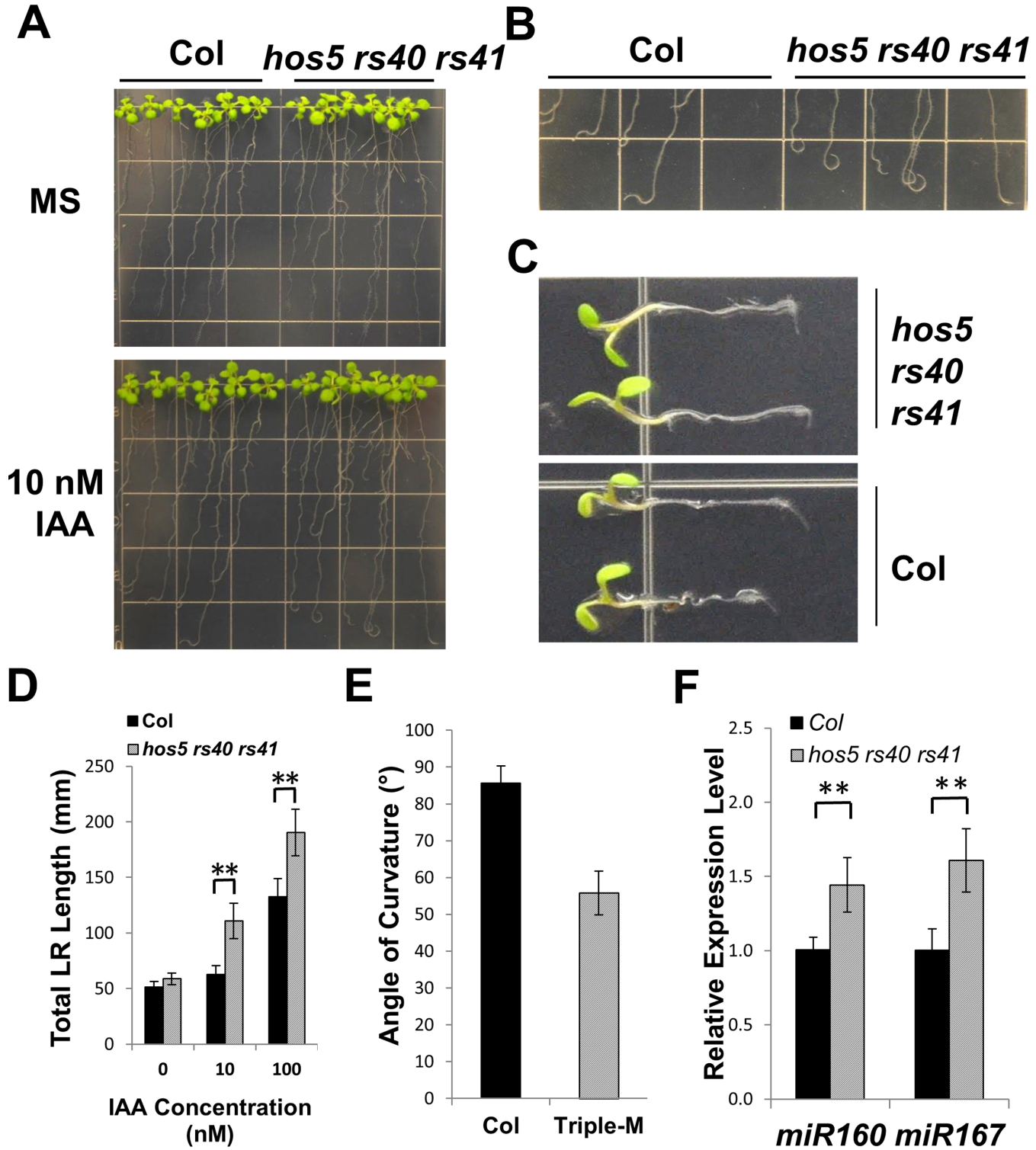

Figure 7. *hos5 rs40 rs41* is hypersensitive to auxin. (**A**) Lateral root and root curling phenotypes of *hos5 rs40 rs41* mutant seedlings. Five-day-old Col (wild-type) and *hos5 rs40 rs41* seedlings were transferred from MS media to MS media or MS media supplemented with 10 nM IAA and plates were placed vertically. Photos were taken 7 days after transfer. (**B**) Enlarged image of roots on 10 nM IAA plate shows the root curling phenotype of the triple mutant after the plate being placed horizontally for 2 days. (**C**) Root gravitropism phenotype of *hos5 rs40 rs41* mutant seedlings. Five-day-old Col and *hos5 rs40 rs41* seedlings were transferred to the MS agar plate and then reoriented by 90°. The picture was taken 12 h after reorientation. (**D**) Quantitative data of auxin response in the *hos5 rs40 rs41* triple mutant. Five-day-old Col and *hos5 rs40 rs41* seedlings were transferred from MS-agar medium to MS medium containing 0, 10 and 100 nM IAA. Lateral root length was measured 7 days after the transfer. Data are means and standard errors ($n = 20$). Asterisks indicate a significant difference between the indicated samples (t-test, $^{**}P < 0.01$). (**E**) The angle of root curvature of seedlings shown in (C). Data represent the mean and standard error ($n = 20$). Triple-M, the *hos5 rs40 rs41* triple mutant. (**F**) The relative expression level of miRNA in the wild-type (Col) and *hos5 rs40 rs41* seedlings, measured by microRNA stem-loop quantitative RT-PCR. Error bars represent the standard deviation ($n = 6$). Asterisks indicate a significant difference between the indicated samples (t-test, $^{**}P < 0.01$).

cating an increased gravitropic response of the triple mutant. Thus, we tested the gravitropic response in the triple mutant by growing seedlings on vertically oriented plates and then reorienting the plates by 90°. The angle of root curvature was recorded 12 h after the reorientation. Roots of the *hos5 rs40 rs41* triple mutant almost fully reoriented to the new gravity direction, while the roots of wild-type seedlings responded to gravity more slowly (Figure 7C and E). This indicates a stronger gravity response and likely increased sensitivity to auxin in the triple mutants compared to the wild-type. Quantitative measurements of total lateral root length and fresh weight of wild-type and triple mutant under IAA treatments indicated that the *hos5 rs40 rs41* triple mutant had significantly increased total lateral root length and fresh weight compared with the wild-type (Figure 7D and Supplementary Figure S9A), consistent with an increased sensitivity of the triple mutant to auxin.

To explore the molecular mechanisms for the increased auxin response in the mutant, we checked the level of auxin-related miRNAs, such as miR160 and miR167, in the mutant. As shown in Figure 7F, the expression levels of these microRNAs increased in *hos5 rs40 rs41*. In contrast, their targeted genes including, *ARF6*, *ARF8*, *ARF10*, *ARF16* and *ARF17*, are repressed in the triple mutant (Supplementary Figure S9B). Consistent with a higher level of miR160, the phenotypes of the triple mutant (Figure 7A) resembled those of plants overexpressing miRNA 160 (50).

HOS5, RS40 and RS41 bind pri-miRNA *in vivo*

To further understand the mechanisms of the HOS5 regulation of miRNA biogenesis, we performed RNA-IP to test if HOS5, RS40 and RS41 can directly bind to pri-miRNA *in vivo*. Seedlings of four transgenic plant lines, HOS5 OX C24, HOS5 OX *fry2–1*, RS40 OX C24 and RS41 OX C24, were harvested and subjected to cross-link by using formaldehyde. Anti-FLAG M_2 beads were used to precipitate protein–RNA complexes. pri-miRNAs were detected by real-time RT-PCR and *ACT2* was used as a negative control. We included pri-miRNAs for miR160 and miR167 that regulate auxin responses (see above) in the investigation. As shown in Figure 8, pri-miRNA160a, pri-miRNA167a and pri-miRNA827 were enriched by immunoprecipitation in HOS5 OX C24. Notably, none of the three pri-miRNAs could be enriched in HOS5 OX *fry2–1*, indicating that the pri-miRNA binding activity of HOS5 requires FRY2, likely via the FRY2-regulated phosphorylation status of HOS5. In RS40 OX C24 and RS41 OX C24, all three pri-miRNAs were enriched, demonstrating that both splicing factors, RS40 and RS41, can bind these pri-miRNAs *in vivo*.

It should be pointed out that, we selected pri-miR160a and pri-miR167a as targets, not only because they are auxin-related pri-miRNAs, but also because they are two different types of pri-miRNA. As tested before, pri-miR160a contains one intron whereas pri-miR167a does not have an intron (48). HOS5, RS40 and RS41 can bind both pri-miRNAs, suggesting that these proteins may affect miRNA biogenesis independently of splicing.

DISCUSSION

HOS5, RS40 and RS41 play an important role in the splicing of a subset of pre-mRNA (44). In this study, we demonstrated that these proteins are also involved in miRNA biogenesis, with their loss of function resulting in altered accumulation of many miRNA (Figure 4). Inaccurate strand selection also occurred in certain miRNA loci (Figure 3). Our previous study revealed that all of these proteins interact with FRY2 (44), which is also involved in miRNA biogenesis by regulating HYL1 phosphorylation (14). In this study, we demonstrated that HOS5 is dephosphorylated by FRY2 (Figure 1). Importantly, we found that the subnuclear localization of both HOS5 and HYL1 is regulated by the phosphorylation status of these proteins. In the *fry2* mutant, HOS5 became more diffuse and was found in far fewer nuclear speckles than in the wild-type (Figure 1). Similarly, fewer HYL1 nuclear bodies were found in the *fry2* mutant (Supplementary Figure S2B and S2C). In both cases, treatment with the protein kinase inhibitor strauosphorine restored the wild-type localization of HOS5 and HYL1 in the *fry2* mutant. Recent studies have implicated that correct subcellular localization of HYL1 protein or its truncated dsRNA-binding domains correlated with their function in miRNA biogenesis (9,51). Thus, it is likely that the changed subnuclear localization of miRNA biogenesis-related proteins in *fry2* may have a major impact on the functions of these proteins in miRNA biogenesis.

The fact that HOS5, RS40, RS40 and FRY2 interact in the nuclear splicing speckles and affect pre-mRNA splicing (44) raises an intriguing question regarding the relationship between splicing and miRNA biogenesis. Using affinity purification and fractionation, components of the spliceosome and the Microprocessor in mammalian cells were found to co-localize (52), suggesting a potential functional relatedness between the two processes. Indeed, several studies have shown that splicing-related proteins or splicing factors are involved in miRNA or siRNA biogenesis (29,53,54) although the mechanism has been unclear. In principle, splicing factors or splicing may affect miRNA biogenesis either indirectly through regulating the expression or the splicing of pri-mRNA biogenesis factors or intron-containing pri-miRNAs, or directly by participating in miRNA biogenesis independently of the splicing activity. Evidence for both direct (53) and indirect (54) involvement of splicing factors in small RNA biogenesis has been reported in other systems. Here, we showed that Arabidopsis HOS5, RS40 and RS41 affects miRNA biogenesis. Our experimental evidence suggests a direct role of these proteins in regulating the biogenesis of a subset of miRNA, although they may also play an indirect role in the biogenesis of some other miRNA.

Unlike in animals, in which the majority of miRNA genes are in introns, most Arabidopsis miRNA loci are encoded by independent transcription units. Although there has been no systematic survey of the intron-containing miRNA genes in Arabidopsis, examination of 20 miRNA genes found that 12 have introns (48). In this study, we found that *hos5* and the SR mutants had splicing defects in processing certain intron-containing pri-miRNAs (Figure 5), yet there was no clear change in splicing for the other intron-containing miRNA genes examined. There was no

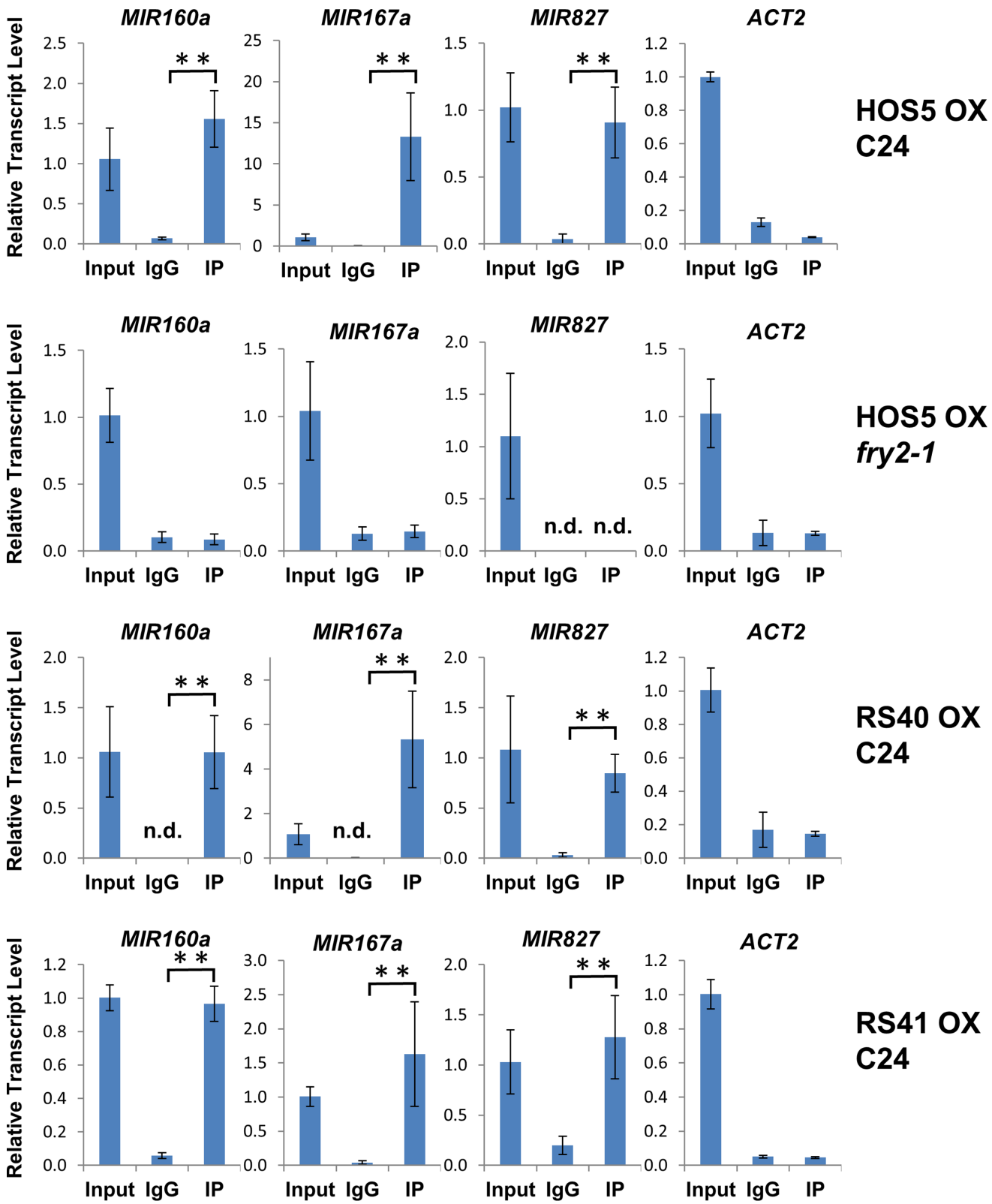

Figure 8. HOS5, RS40 and RS41 bind to pri-miRNA *in vivo*. Four transgenic plants, HOS5 OX C24, HOS5 OX *fry2–1*, RS40 OX C24 and RS41 OX C24, were subject to RNA immunoprecipitation. The levels of pri-miRNA160a, pri-miRNA167a, pri-miRNA827 and *ACT2* in input fraction (input), IgG beads immunoprecipitation (IgG), anti-FLAG M2 beads immunoprecipitation (IP) were detected by quantitative real-time RT-PCR. IgG beads immunoprecipitation was used as a negative control for immunoprecipitation. *ACT2* was used as a quantitative real-time RT-PCR control. Error bars represent standard deviations ($n = 6$). Asterisks indicate a significant difference between the indicated samples (t-test, $^{**}P < 0.01$). n.d., not detectable.

consistent correlation between splicing defects and mature miRNA levels. Furthermore, no obvious defects in the splicing of major miRNA biogenesis genes were observed in the mutants. The expression level of several miRNA biogenesis genes including *DCL1*, *SE*, *CBP20* and *HEN1* was reduced in the mutants, yet others showed no significant changes (Supplementary Figure S7). Reduced expression of genes such as *DCL1* may lead to reduced miRNA production. Thus, these splicing-related proteins may play an indirect role in regulating the biogenesis of some miRNA through regulation of the splicing of miRNA biogenesis genes or pri-miRNA or by regulating the expression of miRNA biogenesis genes.

Consistent with their role in regulating miRNA biogenesis, HOS5, RS40 and RS41 all bind specifically to pri-miRNA *in viv*o (Figure 8). Interestingly, the binding of pri-miRNA by HOS5 requires FRY2, as indicated by the failed binding in the *fry2* mutant background. In this case, FRY2 may function either through dephosphorylating HOS5 (Figure 1A) or by regulating the physical localization or recruitment of HOS5 as a result of the change in its phosphorylation status (Figure 1C) (44), thereby affecting the binding and subsequent processing of pri-miRNA. These possibilities will have to be tested in future studies. It should be noted that these pri-miRNAs that were bound by HOS5 and the SR proteins either contained introns (e.g. pri-miR160a) or did not (pri-miR167a). Thus, the pri-miRNA-binding ability of HOS5 and the SR proteins is independent of the splicing process, pointing to a direct role of these proteins in miRNA biogenesis.

The fact that all of these proteins (HOS5, RS40 and RS41) interact with the core miRNA biogenesis proteins HYL1 and SE in splicing speckles (Figure 2) also strongly supports a direct role for splicing-related factors in the biogenesis of a relatively larger number of miRNA including those that may be indirectly regulated by these splicing related proteins. It is tempting to speculate that these splicing-related proteins may be part of the plant Microprocessor. Due to their RNA-binding ability, these splicing factor proteins and the core miRNA biogenesis proteins, such as HYL1 and SE, may promote each other's recruitment via common RNA structure recognition and protein–protein interaction to the splicing/Microprocessor sites; they may function independently, yet cooperatively, both in pre-mRNA splicing and miRNA biogenesis of a subset of transcripts.

Recently, increasing evidence suggests that miRNA processing defects and mRNA processing defects may occur concurrently in the same mutants (28,29,55), although the detailed mechanism for the linkage remains incompletely understood. Here, we have demonstrated that the three splicing-related proteins HOS5, RS40 and RS41 are directly involved in miRNA biogenesis by binding pri-miRNA and interacting with core miRNA biogenesis components. Further investigation of the detailed mechanisms and functions of these interactions will close the gap between splicing and miRNA processing in the miRNA biogenesis models recently proposed (14,56).

SUPPLEMENTARY DATA

Supplementary Data are available at NAR Online.

FUNDING

Funding for open access charge: Baseline funding provided by the University [BAS/1/1007-01-01].
Conflict of interest statement. None declared.

REFERENCES

1. Voinnet,O. (2009) Origin, biogenesis, and activity of plant microRNAs. *Cell*, **136**, 669–687.
2. Ha,M. and Kim,V.N. (2014) Regulation of microRNA biogenesis. *Nat. Rev. Mol. Cell Biol.*, **15**, 509–524.
3. Lee,Y., Ahn,C., Han,J., Choi,H., Kim,J., Yim,J., Lee,J., Provost,P., Radmark,O., Kim,S. *et al.* (2003) The nuclear RNase III Drosha initiates microRNA processing. *Nature*, **425**, 415–419.
4. Bernstein,E., Caudy,A.A., Hammond,S.M. and Hannon,G.J. (2001) Role for a bidentate ribonuclease in the initiation step of RNA interference. *Nature*, **409**, 363–366.
5. Park,W., Li,J., Song,R., Messing,J. and Chen,X. (2002) CARPEL FACTORY, a Dicer homolog, and HEN1, a novel protein, act in microRNA metabolism in *Arabidopsis thaliana*. *Curr. Biol.*, **12**, 1484–1495.
6. Kurihara,Y. and Watanabe,Y. (2004) Arabidopsis micro-RNA biogenesis through Dicer-like 1 protein functions. *Proc. Natl. Acad. Sci. U.S.A.*, **101**, 12753–12758.
7. Han,M.H., Goud,S., Song,L. and Fedoroff,N. (2004) The Arabidopsis double-stranded RNA-binding protein HYL1 plays a role in microRNA-mediated gene regulation. *Proc. Natl. Acad. Sci. U.S.A.*, **101**, 1093–1098.
8. Song,L., Han,M.H., Lesicka,J. and Fedoroff,N. (2007) Arabidopsis primary microRNA processing proteins HYL1 and DCL1 define a nuclear body distinct from the Cajal body. *Proc. Natl. Acad. Sci. U.S.A.*, **104**, 5437–5442.
9. Wu,F., Yu,L., Cao,W., Mao,Y., Liu,Z. and He,Y. (2007) The N-terminal double-stranded RNA binding domains of Arabidopsis HYPONASTIC LEAVES1 are sufficient for pre-microRNA processing. *Plant Cell*, **19**, 914–925.
10. Fang,Y. and Spector,D.L. (2007) Identification of nuclear dicing bodies containing proteins for microRNA biogenesis in living Arabidopsis plants. *Curr. Biol.*, **17**, 818–823.
11. Grigg,S.P., Canales,C., Hay,A. and Tsiantis,M. (2005) SERRATE coordinates shoot meristem function and leaf axial patterning in Arabidopsis. *Nature*, **437**, 1022–1026.
12. Yang,L., Liu,Z., Lu,F., Dong,A. and Huang,H. (2006) SERRATE is a novel nuclear regulator in primary microRNA processing in Arabidopsis. *Plant J.*, **47**, 841–850.
13. Ren,G., Xie,M., Dou,Y., Zhang,S., Zhang,C. and Yu,B. (2012) Regulation of miRNA abundance by RNA binding protein TOUGH in Arabidopsis. *Proc. Natl. Acad. Sci. U.S.A.*, **109**, 12817–12821.
14. Manavella,P.A., Hagmann,J., Ott,F., Laubinger,S., Franz,M., Macek,B. and Weigel,D. (2012) Fast-forward genetics identifies plant CPL phosphatases as regulators of miRNA processing factor HYL1. *Cell*, **151**, 859–870.
15. Yu,B., Yang,Z., Li,J., Minakhina,S., Yang,M., Padgett,R.W., Steward,R. and Chen,X. (2005) Methylation as a crucial step in plant microRNA biogenesis. *Science*, **307**, 932–935.
16. Zhao,Y., Yu,Y., Zhai,J., Ramachandran,V., Dinh,T.T., Meyers,B.C., Mo,B. and Chen,X. (2012) The Arabidopsis nucleotidyl transferase HESO1 uridylates unmethylated small RNAs to trigger their degradation. *Curr. Biol.*, **22**, 689–694.
17. Zhan,X., Wang,B., Li,H., Liu,R., Kalia,R.K., Zhu,J.K. and Chinnusamy,V. (2012) Arabidopsis proline-rich protein important for development and abiotic stress tolerance is involved in microRNA biogenesis. *Proc. Natl. Acad. Sci. U.S.A.*, **109**, 18198–18203.
18. Wu,X., Shi,Y., Li,J., Xu,L., Fang,Y., Li,X. and Qi,Y. (2013) A role for the RNA-binding protein MOS2 in microRNA maturation in Arabidopsis. *Cell Res.*, **23**, 645–657.
19. Wang,L., Song,X., Gu,L., Li,X., Cao,S., Chu,C., Cui,X., Chen,X. and Cao,X. (2013) NOT2 proteins promote polymerase II-dependent

transcription and interact with multiple MicroRNA biogenesis factors in Arabidopsis. *Plant Cell*, **25**, 715–727.
20. Gregory,B.D., O'Malley,R.C., Lister,R., Urich,M.A., Tonti-Filippini,J., Chen,H., Millar,A.H. and Ecker,J.R. (2008) A link between RNA metabolism and silencing affecting Arabidopsis development. *Dev. Cell*, **14**, 854–866.
21. Kim,S., Yang,J.Y., Xu,J., Jang,I.C., Prigge,M.J. and Chua,N.H. (2008) Two cap-binding proteins CBP20 and CBP80 are involved in processing primary MicroRNAs. *Plant Cell Physiol.*, **49**, 1634–1644.
22. Zhang,S., Liu,Y. and Yu,B. (2014) PRL1, an RNA-binding protein, positively regulates the accumulation of miRNAs and siRNAs in Arabidopsis. *PLoS Genet.*, **10**, e1004841.
23. Zhang,S., Xie,M., Ren,G. and Yu,B. (2013) CDC5, a DNA binding protein, positively regulates posttranscriptional processing and/or transcription of primary microRNA transcripts. *Proc. Natl. Acad. Sci. U.S.A.*, **110**, 17588–17593.
24. Speth,C., Willing,E.M., Rausch,S., Schneeberger,K. and Laubinger,S. (2013) RACK1 scaffold proteins influence miRNA abundance in Arabidopsis. *Plant J.*, **76**, 433–445.
25. Lu,C. and Fedoroff,N. (2000) A mutation in the Arabidopsis HYL1 gene encoding a dsRNA binding protein affects responses to abscisic acid, auxin, and cytokinin. *Plant Cell*, **12**, 2351–2366.
26. Hugouvieux,V., Kwak,J.M. and Schroeder,J.I. (2001) An mRNA cap binding protein, ABH1, modulates early abscisic acid signal transduction in Arabidopsis. *Cell*, **106**, 477–487.
27. Kuhn,J.M., Boisson-Dernier,A., Dizon,M.B., Maktabi,M.H. and Schroeder,J.I. (2006) The protein phosphatase AtPP2CA negatively regulates abscisic acid signal transduction in Arabidopsis, and effects of *abh1* on *AtPP2CA* mRNA. *Plant Physiol.*, **140**, 127–139.
28. Laubinger,S., Sachsenberg,T., Zeller,G., Busch,W., Lohmann,J.U., Ratsch,G. and Weigel,D. (2008) Dual roles of the nuclear cap-binding complex and SERRATE in pre-mRNA splicing and microRNA processing in *Arabidopsis thaliana*. *Proc. Natl. Acad. Sci. U.S.A.*, **105**, 8795–8800.
29. Raczynska,K.D., Stepien,A., Kierzkowski,D., Kalak,M., Bajczyk,M., McNicol,J., Simpson,C.G., Szweykowska-Kulinska,Z., Brown,J.W. and Jarmolowski,A. (2014) The SERRATE protein is involved in alternative splicing in *Arabidopsis thaliana*. *Nucleic Acids Res.*, **42**, 1224–1244.
30. Lee,B.H., Kapoor,A., Zhu,J. and Zhu,J.K. (2006) STABILIZED1, a stress-upregulated nuclear protein, is required for pre-mRNA splicing, mRNA turnover, and stress tolerance in Arabidopsis. *Plant Cell*, **18**, 1736–1749.
31. Ben Chaabane,S., Liu,R., Chinnusamy,V., Kwon,Y., Park,J.H., Kim,S.Y., Zhu,J.K., Yang,S.W. and Lee,B.H. (2013) STA1, an Arabidopsis pre-mRNA processing factor 6 homolog, is a new player involved in miRNA biogenesis. *Nucleic Acids Res.*, **41**, 1984–1997.
32. Koster,T., Meyer,K., Weinholdt,C., Smith,L.M., Lummer,M., Speth,C., Grosse,I., Weigel,D. and Staiger,D. (2014) Regulation of pri-miRNA processing by the hnRNP-like protein AtGRP7 in Arabidopsis. *Nucleic Acids Res.*, **42**, 9925–9936.
33. Bielewicz,D., Kalak,M., Kalyna,M., Windels,D., Barta,A., Vazquez,F., Szweykowska-Kulinska,Z. and Jarmolowski,A. (2013) Introns of plant pri-miRNAs enhance miRNA biogenesis. *EMBO Rep.*, **14**, 622–628.
34. Schwab,R., Speth,C., Laubinger,S. and Voinnet,O. (2013) Enhanced microRNA accumulation through stemloop-adjacent introns. *EMBO Rep.*, **14**, 615–621.
35. Xiong,L., Ishitani,M., Lee,H. and Zhu,J.K. (1999) HOS5-a negative regulator of osmotic stress-induced gene expression in *Arabidopsis thaliana*. *Plant J.*, **19**, 569–578.
36. Xiong,L., Lee,H., Ishitani,M., Tanaka,Y., Stevenson,B., Koiwa,H., Bressan,R.A., Hasegawa,P.M. and Zhu,J.K. (2002) Repression of stress-responsive genes by FIERY2, a novel transcriptional regulator in Arabidopsis. *Proc. Natl. Acad. Sci. U.S.A.*, **99**, 10899–10904.
37. Nakagawa,T., Kurose,T., Hino,T., Tanaka,K., Kawamukai,M., Niwa,Y., Toyooka,K., Matsuoka,K., Jinbo,T. and Kimura,T. (2007) Development of series of gateway binary vectors, pGWBs, for realizing efficient construction of fusion genes for plant transformation. *J. Biosci. Bioeng.*, **104**, 34–41.
38. Earley,K.W., Haag,J.R., Pontes,O., Opper,K., Juehne,T., Song,K. and Pikaard,C.S. (2006) Gateway-compatible vectors for plant functional genomics and proteomics. *Plant J.*, **45**, 616–629.
39. Nakagawa,T., Suzuki,T., Murata,S., Nakamura,S., Hino,T., Maeo,K., Tabata,R., Kawai,T., Tanaka,K., Niwa,Y. *et al.* (2007) Improved Gateway binary vectors: high-performance vectors for creation of fusion constructs in transgenic analysis of plants. *Biosci. Biotech. Biochem.*, **71**, 2095–2100.
40. Varkonyi-Gasic,E., Wu,R., Wood,M., Walton,E.F. and Hellens,R.P. (2007) Protocol: a highly sensitive RT-PCR method for detection and quantification of microRNAs. *Plant Methods*, **3**, 12.
41. Wang,L., Feng,Z., Wang,X., Wang,X. and Zhang,X. (2010) DEGseq: an R package for identifying differentially expressed genes from RNA-seq data. *Bioinformatics*, **26**, 136–138.
42. Trapnell,C., Pachter,L. and Salzberg,S.L. (2009) TopHat: discovering splice junctions with RNA-Seq. *Bioinformatics*, **25**, 1105–1111.
43. Trapnell,C., Williams,B.A., Pertea,G., Mortazavi,A., Kwan,G., van Baren,M.J., Salzberg,S.L., Wold,B.J. and Pachter,L. (2010) Transcript assembly and quantification by RNA-Seq reveals unannotated transcripts and isoform switching during cell differentiation. *Nat. Biotechnol.*, **28**, 511–515.
44. Chen,T., Cui,P., Chen,H., Ali,S., Zhang,S. and Xiong,L. (2013) A KH-domain RNA-binding protein interacts with FIERY2/CTD phosphatase-like 1 and splicing factors and is important for pre-mRNA splicing in Arabidopsis. *PLoS Genet.*, **9**, e1003875.
45. Kinoshita,E., Takahashi,M., Takeda,H., Shiro,M. and Koike,T. (2004) Recognition of phosphate monoester dianion by an alkoxide-bridged dinuclear zinc(II) complex. *Dalton Trans.*, 1189–1193.
46. Yoo,S.D., Cho,Y.H. and Sheen,J. (2007) Arabidopsis mesophyll protoplasts: a versatile cell system for transient gene expression analysis. *Nat. Protoc.*, **2**, 1565–1572.
47. Koroleva,O.A., Calder,G., Pendle,A.F., Kim,S.H., Lewandowska,D., Simpson,C.G., Jones,I.M., Brown,J.W. and Shaw,P.J. (2009) Dynamic behavior of Arabidopsis eIF4A-III, putative core protein of exon junction complex: fast relocation to nucleolus and splicing speckles under hypoxia. *Plant Cell*, **21**, 1592–1606.
48. Szarzynska,B., Sobkowiak,L., Pant,B.D., Balazadeh,S., Scheible,W.R., Mueller-Roeber,B., Jarmolowski,A. and Szweykowska-Kulinska,Z. (2009) Gene structures and processing of *Arabidopsis thaliana* HYL1-dependent pri-miRNAs. *Nucleic Acids Res.*, **37**, 3083–3093.
49. Lopato,S., Waigmann,E. and Barta,A. (1996) Characterization of a novel arginine/serine-rich splicing factor in Arabidopsis. *Plant Cell*, **8**, 2255–2264.
50. Turner,M., Nizampatnam,N.R., Baron,M., Coppin,S., Damodaran,S., Adhikari,S., Arunachalam,S.P., Yu,O. and Subramanian,S. (2013) Ectopic expression of miR160 results in auxin hypersensitivity, cytokinin hyposensitivity, and inhibition of symbiotic nodule development in soybean. *Plant Physiol.*, **162**, 2042–2055.
51. Liu,Q., Yan,Q., Liu,Y., Hong,F., Sun,Z., Shi,L., Huang,Y. and Fang,Y. (2013) Complementation of HYPONASTIC LEAVES1 by double-strand RNA-binding domains of DICER-LIKE1 in nuclear dicing bodies. *Plant Physiol.*, **163**, 108–117.
52. Kataoka,N., Fujita,M. and Ohno,M. (2009) Functional association of the Microprocessor complex with the spliceosome. *Mol. Cell. Biol.*, **29**, 3243–3254.
53. Bayne,E.H., Portoso,M., Kagansky,A., Kos-Braun,I.C., Urano,T., Ekwall,K., Alves,F., Rappsilber,J. and Allshire,R.C. (2008) Splicing factors facilitate RNAi-directed silencing in fission yeast. *Science*, **322**, 602–606.
54. Kallgren,S.P., Andrews,S., Tadeo,X., Hou,H., Moresco,J.J., Tu,P.G., Yates,J.R. 3rd, Nagy,P.L. and Jia,S. (2014) The proper splicing of RNAi factors is critical for pericentric heterochromatin assembly in fission yeast. *PLoS Genet.*, **10**, e1004334.
55. Raczynska,K.D., Simpson,C.G., Ciesiolka,A., Szewc,L., Lewandowska,D., McNicol,J., Szweykowska-Kulinska,Z., Brown,J.W. and Jarmolowski,A. (2010) Involvement of the nuclear cap-binding protein complex in alternative splicing in *Arabidopsis thaliana*. *Nucleic Acids Res.*, **38**, 265–278.
56. Rogers,K. and Chen,X. (2013) Biogenesis, turnover, and mode of action of plant microRNAs. *Plant Cell*, **25**, 2383–2399.